data demonstrated that the heterogenous washout of ^{99m}Tc-ECD within 60 min could be negligible (Flores L II, *personal communication*). The influence of inhomogeneous washout of the tracer is thought to be small in our ^{99m}Tc-ECD SPECT protocol.

CONCLUSION

The vasodilatory capacity under acetazolamide challenge was underestimated with ^{99m}Tc-ECD when compared to ^{123}I-IMP. However, this underestimation could be corrected by the PS model. Technetium-99m-ECD SPECT that is corrected based on the PS model may be a useful method for evaluating cerebrovascular reserve using acetazolamide challenge.

REFERENCES

1. Kung HF, Ohmomo Y, Kung MP. Current and future radiopharmaceuticals for brain imaging with single-photon emission computed tomography. *Semin Nucl Med* 1990; 20:290–302.
2. Greenberg JH, Lassen NA. Characterization of ^{99m}Tc bicisate as an agent for the measurement of cerebral blood flow with SPECT. *J Cereb Blood Flow and Metabol* 1994;14(suppl 1):S1–S3.
3. Knudsen GM, Anderson AR, Sommier FE, et al. Brain extraction and distribution of ^{99m}Tc bicisate in humans and in rats. *J Cereb Blood Flow and Metabol* 1994;14(suppl 1):S12–S18.
4. Yonekura Y, Tsuchida T, Sadato N, et al. Brain perfusion SPECT with ^{99m}Tc bicisate: comparison with PET measurement and linearization based on permeability-surface area product model. *J Cereb Blood Flow and Metabol* 1994;14(suppl 1):S58–S65.
5. Shishido F, Uemura K, Murakami M, et al. Cerebral uptake of ^{99m}Tc bicisate in patients with cerebrovascular disease in comparison with CBF and CMRO2 measured by positron emission tomography. *J Cereb Blood Flow and Metabol* 1994;14(suppl 1):S66–S75.
6. Nakagawara J, Nakamura J, Takeda R, et al. Assessment of postischemic reperfusion and diamox activation test in stroke using ^{99m}Tc-ECD SPECT. *J Cereb Blood Flow and Metabol* 1994;14(suppl 1):S49–S57.
7. Friberg L, Anderson AR, Lassen NA, et al. Retention of ^{99m}Tc bicisate in the human brain after intracarotid injection. *J Cereb Blood Flow and Metabol* 1994;14(suppl 1):S19–S27.
8. Vorstrup S. Tomographic cerebral blood flow measurements in patients with ischemic cerebrovascular disease, and evaluation of the vasodilatory capacity by the acetazolamide test. *Acta Neurol Scand* 1988;77:5–48.
9. Vorstrup S, Brun B, Lassen NA. Evaluation of the cerebral vasodilatory capacity by the acetazolamide test before EC-IC bypass surgery in patients with occlusion of the internal carotid artery. *Stroke* 1986;17:1291–1298.
10. Hirano T, Minematsu K, Hasegawa Y, et al. Acetazolamide reactivity on I-123 IMP single-photon emission computed tomography in patients with major cerebral artery occlusive disease: correlation with positron emission tomography parameters. *J Cereb Blood Flow Metabol* 1994;14:763–770.
11. Yamashita T, Hayashi M, Kashiwagi S, et al. Cerebrovascular reserve capacity in ischemia due to occlusion of major arterial trunk: studies by Xe-CT and the acetazolamide test. *J Comput Assist Tomogr* 1992;16:750–755.
12. Moretti JL, Caglar M, Weinmann P. Cerebral perfusion imaging tracers for SPECT: which one to choose? *J Nucl Med* 1995;36:359–363.
13. Walovitch RC, Hill TC, Garrity ST, et al. Characterization ^{99m}Tc-L,L-ECD for brain perfusion imaging, part 1: pharmacology of ^{99m}Tc-ECD in nonhuman primates. *J Nucl Med* 1989;30:1892–1901.
14. Lassen NA, Anderson AR, Friberg L, et al. The retention of ^{99m}Tc d, l-HMPAO in the human brain after intracarotid bolus injection: a kinetic analysis. *J Cereb Blood Flow and Metabol* 1988;8:S13–S22.
15. Inugami A, Kanno I, Uemura K, et al. Linearization correction of ^{99m}Tc-labeled hexamethyl-propylene amine oxime (HMPAO) image in terms of regional CBF distribution: comparison to C15 O2 inhalation steady-state method measured by positron emission tomography. *J Cereb Blood Flow and Metabol* 1988;8:S52–S60.
16. Yonekura Y, Nishizawa S, Mukai T, et al. SPECT with ^{99m}Tc d,l-hexamethylpropylene amine oxime (HMPAO) compared with regional cerebral blood flow measured by PET: effects of linearization. *J Cereb Blood Flow and Metabol* 1988;8:S82–S89.
17. Léveillé J, Demonceau G, Walovitch RC. Intersubject comparison between ^{99m}Tc-ECD and ^{99m}Tc-HMPAO in healthy human subjects. *J Nucl Med* 1992;33:1902–1910.
18. Murase K, Tanada S, Inoue T, et al. Kinetic behavior of ^{99m}Tc-ECD in the human brain using compartment analysis and dynamic SPECT: comparison with ^{99m}Tc-HMPAO [Abstract]. *J Nucl Med* 1992;33:909.
19. Kuhl DE, Barrio JR, Huang SC, et al. Quantifying local cerebral blood flow by N isopropyl p 123 iodoamphetamine (IMP) tomography. *J Nucl Med* 1982;23:196–203.
20. Hashikawa K, Matsumoto M, Moriwaki H, et al. Split-dose ^{123}I-IMP SPECT: sequential quantitative regional cerebral blood flow change with pharmacological intervention. *J Nucl Med* 1994;35:1226–1233.
21. Holm S, Madsen PL, Sperling B, et al. Use of ^{99m}Tc bicisate in activation studies by split-dose technique. *J Cereb Blood Flow and Metabol* 1994;14(suppl 1):S115–S120.
22. Moretti JL, Tamgac F, Weinmann P, et al. Early and delayed brain SPECT with ^{99m}Tc-ECD and ^{123}I-IMP in subacute strokes. *J Nucl Med* 1994;35:1444–1449.

Viable Neurons with Luxury Perfusion in Hydrocephalus

Ching-yee Oliver Wong, Mark G. Luciano, William J. MacIntyre, Richard C. Brunken, Joseph F. Hahn and Raymundo T. Go

Departments of Nuclear Medicine and Neurosurgery, The Cleveland Clinic Foundation, Cleveland, Ohio

A woman with hydrocephalus due to aqueductal stenosis had functional imaging of cerebral perfusion and metabolism to demonstrate the effects of endoscopic third ventriculostomy–a new form of internal surgical shunting. Technetium-99m-ECD SPECT and ^{18}F-FDG PET showed regional luxury perfusion at the left frontal region. Three months after a successful third ventriculostomy, a repeated imaging of cerebral perfusion and metabolism showed resolution of luxury perfusion and global improvement of both perfusion and metabolism. This concurred with postoperative clinical improvement. The paired imaging of cerebral perfusion and metabolism provides more information than just imaging perfusion or metabolism. Thus, the detection of perfusion and metabolism mismatch may open a new window of opportunity for surgical intervention.

Key Words: hydrocephalus; perfusion and metabolism mismatch

J Nucl Med 1997; 38:1467–1470

The link between cellular viability and functional outcome after surgical intervention has been demonstrated in the myocardium with coronary artery disease by imaging myocardial perfusion and metabolism using $^{13}NH_3$ and ^{18}F-FDG (*1*) and by $H_2{}^{15}O$ and ^{11}C-acetate (*2*) PET. Recent studies using ^{123}I-labeled benzodiazepine receptor antagonist (*3–5*) and paired studies with ^{99m}Tc-HMPAO and ^{18}F-FDG (*6*) have opened a new quest into neuronal viability in cerebrovascular disease. However, little is known about neuronal viability and function in hydrocephalus, in which there is net accumulation of cerebrospinal fluid (CSF) within the cerebral ventricles with resultant dilatation (*7*). The constant pressure on cortical cells causes reduction of cerebral perfusion (*8,9*) and metabolism (*10–12*) that can be imaged noninvasively in humans by radionuclide emission tomography such as PET and SPECT. The structural changes are displayed by anatomical imaging such as x-ray CT or MRI as dilatation of ventricular system and thinning of the cortex. It is presumed that irreversible cerebral cortical damage has occurred when ventricles become dilated and metabolism shuts down. Therefore, the viability of the cortical neurons

Received Jul. 29, 1996; revision accepted Oct. 23, 1996.

For correspondence or reprints contact: C. Oliver Wong, MBBS, PhD, Department of Nuclear Medicine, Gb3, The Cleveland Clinic Foundation, Cleveland, OH 44143.

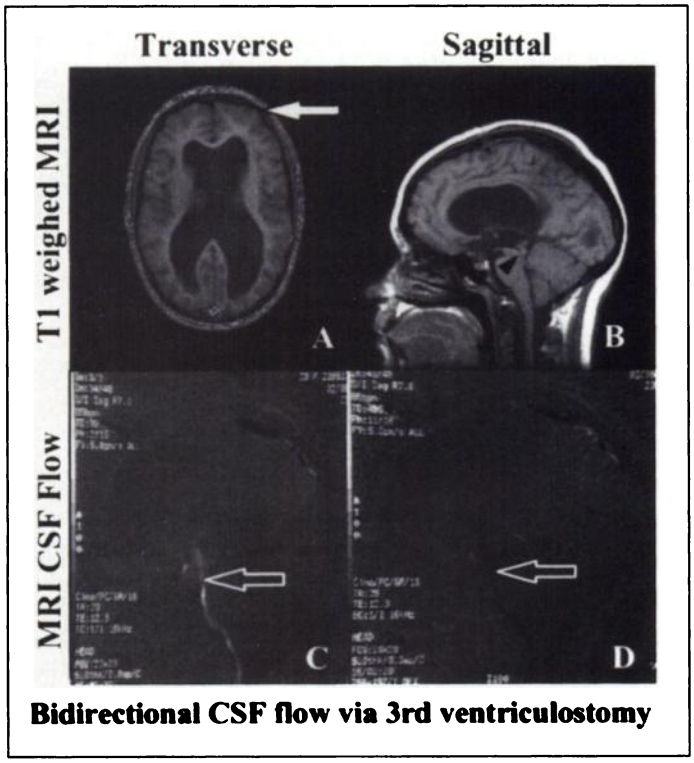

FIGURE 1. (A) Transverse and (B) sagittal T1-weighted MRI images, in a patient with hydrocephalus due to aqueductal stenosis (arrow head), show dilatation of ventricular system. Note the left frontal region shows no remarkable structural changes (solid arrow). (C, D) The CSF flow study after neuroendoscopic third ventriculostomy shows bidirectional CSF flow indicating patent ventriculostomy.

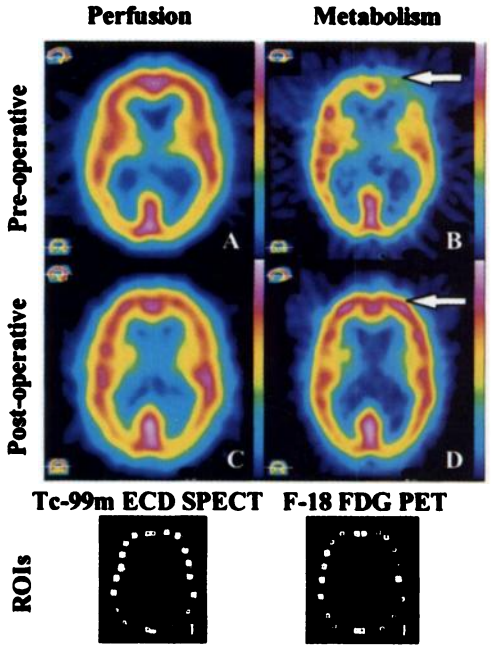

FIGURE 2. (A) Representative transverse ^{99m}Tc-ECD SPECT and (B) ^{18}F-FDG PET images performed before third ventriculostomy show decreased metabolism relative to perfusion at the frontal lobe on the left side of the patient (arrow). The (C) postoperative ^{99m}Tc-ECD SPECT and (D) ^{18}F-FDG PET images show (D) normalization of metabolism relative to (C) perfusion which, together with functional recovery, indicate viable neurons present in the previously observed areas of mismatch metabolism relative to perfusion (luxury perfusion). The twenty 4 × 4-pixel ROIs placed on (A) and (B) are shown in (E) and (F), respectively.

surrounding the dilated ventricles with reduced perfusion or metabolism would be important information for considering surgical shunting procedures such as ventriculo-atrial or -peritoneal shunts or endoscopic third ventriculostomy. Can the neurons in those regions, with reduced perfusion or metabolism that are at risk of damage but still viable, be salvaged?

Previous PET imaging has shown that cerebral perfusion in normal brain tissue is constantly regulated to match metabolic demand (*13,14*) and brain tissue in hydrocephalus with increased cortical oxygen extraction correlated with improvement of cerebral perfusion after surgical shunting (*15*). The neuronal tissue uses glucose exclusively for its energy supply in its usual state (*16*). It is quite possible that a mismatched pattern of perfusion and glucose metabolism would represent a state of viable neurons in crisis, as reported recently in cerebrovascular disease (*6*). We, without cyclotron facilities, used ^{99m}Tc L,L-ethyl cysteinate dimer (ECD) which acts like a chemical microsphere to demonstrate perfusion and ^{18}F 2-fluoro-2-deoxy-D-glucose (FDG) which is a glucose analog to measure glucose metabolism. ECD is lipophilic and neutral which crosses the blood-brain barrier readily and its selective retention in brain tissue is achieved by de-esterification into polar acidic products that are ionized at physiologic pH (*17*). FDG is transported into the cells of most tissues by facilitated diffusion, then phosphorylated into FDG-6-PO_4 and trapped intracellularly (*18,19*). These two tracers are also available commonly for clinical studies in other clinical centers. If neurons with decoupling of perfusion and glucose metabolism due to damaging forces from compression by hydrocephalus are still viable, the relief of pressure by surgical shunting will reverse such decoupling (mismatch) in the dual imaging of cerebral perfusion and metabolism because dead neuronal cells in the central nervous system cannot regenerate. The gold standard, as in coronary revascularization, will be recovery of neuronal function after surgical (external or internal) shunting.

CASE REPORT

A 23-yr-old patient with good past health except for memory problems since high school. She experienced bilateral numbness and weakness of her lower extremities for 2 wk. She also had bilateral frontal headache over the past 4–5 mo. There was no history of urinary incontinence. On physical examination, she was found to have bilateral leg weakness, ataxia and mild impairment of both short- and long-term memory. Her MRI (Figs. 1A and B) revealed hydrocephalus due to aqueductal stenosis. Because of the lack of an objective method for functional assessment of neurologic deficits and effects of third ventriculostomy, a new form of surgical shunting that diverts CSF internally by a neuroendoscopic procedure (*20*), nuclear medicine brain imaging was ordered. Technetium-99m-ECD SPECT imaging (see Appendix for technical details) was first performed to study cerebral perfusion that showed effects of hydrocephalus but no regional defects (Fig. 2A). Fluorine-18-FDG-PET imaging (Appendix) was performed 2 hr later to look for metabolic abnormalities in this patient. It showed a mismatched metabolic defect, most prominent at the left frontal region (Fig. 2B). This is a phenomenon of luxury perfusion or perfusion and metabolic mismatch observed previously in stroke (*21–23*) but it has not been reported in hydrocephalus. The same pair of images was repeated (Appendix) 3 mo after endoscopic third ventriculostomy. The metabolism (Fig. 2D) was improved to

TABLE 1
Asymmetric Index

	Perfusion (F)	Metabolism (F)	Perfusion (NF)	Metabolism (NF)
Pre-operative	−1.03 ± 1.01%	17.48 ± 3.85%	0.27 ± 4.54%	3.86 ± 6.62%
Post-operative	2.97 ± 1.36%	−1.20 ± 6.62%	0.42 ± 6.29%	−2.11 ± 4.37%
Two-tailed p	0.20	0.01	0.95	0.11

F = frontal, NF = nonfrontal brain regions.

match perfusion (Fig. 2C) at the left frontal region and there was no more decoupling (arrows in Figs. 2B and 2D). The anatomical imaging by MRI (Figs. 1C and 1D) revealed exuberant bidirectional flow through the floor of the third ventricle consistent with widely patent third ventriculostomy. There are no changes noted in the ventricular size when compared to preshunting MRI.

In order to detect the global changes in cerebral perfusion and metabolism, the mean and standard deviation of count densities of the entire brain were calculated using the method described previously (*24*). For local quantification, 20 different 4 × 4 pixel ROIs were placed on the transverse images (Figs. 2E and 2F) to extract count densities. All count densities were then normalized to the maximal count in the cerebellum. The cerebellum was chosen as reference region, because the mean regional cerebral perfusion was shown not to be different from normal controls (*25*) and hydrocephalus is not known to be associated with structural abnormalities in the cerebellum. The mean count ratios in cerebral perfusion and metabolism improved significantly, respectively, from 0.80 ± 0.11 and 0.88 ± 0.11 preoperatively to 0.83 ± 0.14 and 0.91 ± 0.12 postoperatively (two-tailed $p < 0.00001$ in both perfusion and metabolism). The asymmetric indices, defined by (Right − Left)/(Right + Left), in the frontal and nonfrontal regions were tabulated in Table 1. The table showed significant reversal of the asymmetric index in frontal metabolism but not in frontal perfusion. This concurred with our visual observation of luxury perfusion, a form of mismatch in perfusion and metabolism. However, although the neurologic symptoms (bilateral leg numbness and weakness, ataxia and frontal headache) that the patient experienced before endoscopic third ventriculostomy were resolved, paralleling the observations in the pre- and postshunting perfusion and metabolic imaging just described, there are no localizing focal neurologic signs or symptoms to relate to the major site of luxury perfusion. Thus, the clinical improvement was most likely related to global improvement of metabolism and perfusion.

DISCUSSION

Quantitative PET studies have demonstrated coupling between cerebral blood flow, oxygen consumption and glucose utilization (*13,14*). Shih et al. (*9*) had demonstrated reversible hypoperfusion in human cerebral cortex after shunting in a single patient with normal pressure hydrocephalus by using a three-dimensional display of ^{99m}Tc-HMPAO cerebral perfusion SPECT images. But the status of metabolism, which might not be coupled to perfusion as illustrated in our case, was unknown. Friedland et al. (*12*) demonstrated reversible hypometabolism in human cerebral cortex after shunting in a single patient with normal pressure hydrocephalus by using ^{18}F-FDG PET images during the management of dementia. However, there were no accompanying perfusion images presented to illustrate perfusion and metabolism mismatch or match. Clearly, the ability of the neurons in a brain region to regain metabolism after surgery but not just perfusion indicates the presence of viable neurons in that particular region. However, reduced metabolism could be due to neuronal cell loss, neurons at crisis (ischemia) or deafferentation (diaschisis). Thus, in order to identify neuronal viability within present facilities of most clinical centers, dual imaging of cerebral perfusion and metabolism in a single day static study to look for perfusion and metabolism mismatches (luxury or misery perfusion) before surgical shunting may be promising, as also suggested by other investigators (*6*). When the ventricular system starts to dilate, compression of cerebral cortical tissue will result in gradual reduction of perfusion and metabolism. However, continued compression of cortical tissue may result in metabolic shut down and the neurons will be on the verge of dying. The perfusion is maintained by reactive hyperemia, a phenomenon of luxury perfusion related to metabolic acidosis (*26*). If nothing is done, the neurons will inevitably succumb to cellular death. Thus, the ability to detect neuronal viability by noninvasive imaging of cerebral perfusion and metabolism opens a window of opportunity for surgical intervention. The detection of perfusion and metabolism decoupling when the neurons are still viable may be quite short in time which, to the best of our knowledge, has not been reported previously in hydrocephalus. Contrary to previous report that the reduction of metabolism is global (*27*), the present case demonstrates also the regional reduction of neuronal metabolism. This information regarding neuronal viability is not available in the present high spatial resolution anatomical imaging such as MRI and CT scans and cannot be recorded by surface electroencephalography, as expected from the hierarchy of neurochemistry (*28*) from metabolism down to perfusion, electrical events, structural changes and/or clinical signs and symptoms. Although imaging in the higher hierarchy with ^{123}I iomazenil appears to be promising in the acute or subacute cerebrovascular disease, it may not be applicable to hydrocephalus as there is evidence that persistently ischemic areas tend to lose benzodiazepine receptors as well (*29*). Current practice of surgical shunting depends on the patient's symptoms and signs together with structural changes by anatomical imaging that occur much later than functional changes in perfusion and metabolism and there are no suitable noninvasive objective method for functional assessment before and after shunting. Although the patient reported has developed symptoms, nuclear imaging still helps to document the effects of endoscopic third ventriculostomy and assess subsequent recovery of function together with clinical observation of symptomatic improvement after surgery, which is the ultimate gold standard of neuronal viability.

CONCLUSION

Although the nuclear imaging combination of perfusion and metabolism is commonly used in myocardial viability, it has not been widely used in neuronal viability. Our observation of cerebral perfusion and metabolic mismatches helps to identify viable neurons that are at risk of damage due to compression by hydrocephalus, and these neurons will be salvageable by surgical shunting. The dual imaging of cerebral perfusion and metabolism potentially would help neurosurgeons decide on a shunting procedure well before the clinical signs or symptoms appear and assess functional recovery objectively. Long-term

follow-up and extension of the study to include more patients are in progress.

APPENDIX

Each pair of images was performed on the same day with ^{99m}Tc-ECD SPECT first, followed by ^{18}F-FDG PET. In the SPECT scan, an average of 738 ± 338 MBq ^{99m}Tc-ECD was injected in a quiet and dimly lit room. SPECT acquisition, lasting for slightly less than 30 min, using a triple detector gamma-camera equipped with a low-energy, ultrahigh resolution parallel-hole collimator (TRIONIX, Twinsburg, OH) in a 128 × 128 matrix (pixel size = 3.56 mm), was started 10–15 min after injection of ^{99m}Tc-ECD. The raw SPECT projection images were reconstructed in a 64 × 64 matrix with the same pixel size of 3.56 mm as in the acquisition and a slice thickness of 3.56 mm, using a uniform attenuation coefficient of 0.11 cm^{-1}, a five-pixel axial smoothing kernel (1 2 5 2 1) and Hanning filter with a Nyquist frequency of 1.404 cycles cm^{-1} and a cutoff frequency of 1.00 cycle cm^{-1}. The pixel size and slice thickness were chosen to have the same size for a symmetrical cubic voxel from the gamma camera used that had a resolution of approximately 7 mm at 10 cm from the collimator. The PET scan was obtained on a Posicam 6.5 PET system (Positron Corporation, Houston, TX) using an average of 165 ± 18 MBq ^{18}F-FDG. The acquisition was initiated at an average of 45 min after injection of the tracer. The axial field of view consisted of 21 contiguous slices with axial thickness of 5.125 mm. The in-plane resolution was 5.8 mm and the axial resolution was 11.9 mm FWHM. Attenuation correction was applied for each slice using separate elliptical ROIs defined interactively by the operator to trace the scalp. A uniform attenuation coefficient of 0.096 cm^{-1} was used. Reconstruction of a 256 × 256 image matrix with a pixel size of 1.71 mm was performed by Positron Data Acquisition System (PDAS, Positron Corporation, Houston, TX) using linear filtered backprojection with a Butterworth filter of order 10 and cutoff frequency of 0.04 cycle/mm. After filtering, the in-plane resolution became 15.5 mm FWHM. Each set of images were then transferred to MicroVAX III computer (Digital Equipment Corporation, Maynard, MA) where they were further processed by reorientation along the same orthogonal axes of the SPECT images, reduced the matrix size to 64 × 64 and summed slices into 2-pixel thickness. In this way, the dimension of a voxel is also cubic, 3.42 mm in size which is very similar to the voxel size in the SPECT images. The images were displayed, scaled conventionally to the maximal pixel counts, in dual tomographic windows for visual comparison (Fig. 2).

REFERENCES

1. Tillisch J, Brunken R, Marshall R, et al. Reversibility of cardiac wall motion abnormalities predicted by positron tomography. *N Engl J Med* 1986;314:884–888.
2. Gropler RJ, Geltman EM, Sampathkumaran K, et al. Functional recovery after coronary revascularization for chronic coronary artery disease is dependent on maintenance of oxidative metabolism. *J Am Coll Cardiol* 1992;20:569–577.
3. Odano I, Miyashita K, Minoshima S, et al. A potential use of a ^{123}I-labeled benzodiazepine receptor antagonist as a predictor of neuronal cell viability: comparisons with ^{14}C-labeled 2-deoxyglucose autoradiography and histopathological examination. *Nucl Med Comm* 1995;16:443–446.
4. Sasaki M, Ichiya Y, Kuwabara Y, et al. Brain benzodiazepine receptor distribution in patients with chronic cerebrovascular disease: a potential probe for evaluation neuronal cell loss [Abstract]. *J Nucl Med* 1996;37:133P–134P.
5. Hayashida K, Miyake Y, Hirose Y, et al. Reduction of ^{123}I-iomazenil uptake in the hemodynamically and metabolically impaired cerebral areas in patients with cerebrovascular disease [Abstract]. *Ann Nuklearmedizin* 1996;10:S66.
6. Meijer RJ, Hasan D, van Peski J, Valkema R, Koudstaal PJ, Krenning EP. Cerebral uptake of ^{18}F-FDG and ^{99m}Tc-HMPAO by SPECT in ischemic stroke [Abstract]. *Eur J Nucl Med* 1996;23:1082.
7. Vick NA, Rottemberg DA. Disorders of intracranial pressure. In: Wyngaarden JB, Smith LH, Bennett JC, eds. *Cecil text book of medicine*. Philadelphia, PA: WB Saunders; 1992:2221–2224.
8. Greitz TVB, Grepe AOL, Kalmer MSL, Lopez J. Pre- and post-operative evaluation of cerebral blood flow in low-pressure hydrocephalus. *J Neurosurg* 1969;31:644–651.
9. Shih WJ, Tasdemiroglu E. Reversible hypoperfusion of the cerebral cortex in normal-pressure hydrocephalus on technetium-99m-HMPAO brain SPECT images after shunt operation. *J Nucl Med* 1995;36:470–473.
10. Grubb RL, Raichle ME, Phelps ME, Ratcheson RA. Effects of increased intracranial pressure on cerebral blood volume, blood flow, and oxygen utilization in monkeys. *J Neurosurg* 1975;43:385–398.
11. Lying-Tunell U, Lindblad BS, Malmlund HO, Persson B. Cerebral blood flow and metabolic rate of oxygen, glucose, lactate, pyruvate, ketone bodies and amino acids. II. Presenile dementia and normal-pressure hydrocephalus. *Acta Neurol Scand* 1981;63:337–350.
12. Friedland R. 'Normal'-pressure hydrocephalus and the saga of the treatable dementias. *JAMA* 1989;262:2577–2581.
13. Frackowiak RSJ, Lenzi GL, Jones T, Heather JD. Quantitative measurement of regional cerebral blood flow and oxygen metabolism in man using ^{15}O and positron emission tomography: theory, procedure and normal values. *J Comp Assist Tomogr* 1980;4:727–736.
14. Baron JC, Rougemont D, Collard P, et al. Coupling between cerebral blood flow, oxygen consumption and glucose utilization: its study with positron tomography. In: Reivich M, Alavi A, eds. *Positron emission tomography*. New York, NY: Alan R Liss; 1985:203–218.
15. Brooks DJ, Beaney RP, Powell M, et al. Studies on cerebral oxygen metabolism, blood flow, and blood volume, in patients with hydrocephalus before and after surgical decompression, using positron emission tomography. *Brain* 1986;109:613–628.
16. Sokoloff L. Cerebral circulation, energy metabolism and protein synthesis: general characteristics and principles of measurement. In: Phelps ME, Mazziotta JC, Schelbert HR, eds. *Positron emission tomography and autoradiography: principles and applications for the brain and heart*. New York, NY: Raven Press; 1986:1–71.
17. Walovitch RC, Franceschi M, Piccard M, et al. Metabolism of ^{99m}Tc-l,l,-ethyl cysteinate dimer in healthy volunteers. *Neuropharm* 1991;30:283–292.
18. Sokoloff L, Reivich M, Kennedy C, et al. The [^{14}C]deoxyglucose method for the measurement of local cerebral glucose utilization: theory, procedure and normal values in the conscious and anaesthetized albino rat. *J Neurochem* 1977;28:897–916.
19. Phelps ME, Huang SC, Hoffman EJ. Tomographic measurements of local cerebral glucose metabolism in humans with [^{18}F]-2-fluoro-2-deoxy-D-glucose: validation of method. *Ann Neurol* 1979;6:371–388.
20. Jones RFC, Stening WA, Brydon M. Endoscopic third ventriculostomy. *Neurosurg* 1990;26:86–92.
21. Devous MD Sr, Stokely EM, Bonte FJ. Quantitative imaging of regional cerebral blood flow in man by dynamic single photon tomography. In: Holman BL, ed. *Radionuclide imaging of the brain*. Edinburgh, Scotland: Churchill Livingstone; 1985:135–162.
22. Hellman RS, Tikofsky RS. An overview of the contributions of regional cerebral blood flow studies in cerebrovascular disease. Is there a role for single-photon emission computed tomography? *Semin Nucl Med* 1990;20:303–324.
23. Alavi A, Hirsch L. Studies of central nervous system disorders with single-photon emission computed tomography and positron emission tomography: evolution over the past two decades. *Semin Nucl Med* 1991;21:58–81.
24. Wong CYO, Geller EB, Chen EQ, et al. Outcome of temporal lobe epilepsy surgery predicted by statistical parametric PET imaging. *J Nucl Med* 1996;37:1094–1100.
25. Waldemar G, Schmidt JF, Delecluse F, Anderson AR, Gjerris F, Paulson OB. High resolution SPECT with ^{99m}Tc-d,l-HMAPO in normal pressure hydrocephalus before and after shunt operation. *J Neurol Neurosurg Psych* 1993;56:655–664.
26. Lassen NA. The luxury-perfusion syndrome and its possible relation to acute metabolic acidosis localized within the brain. *Lancet* 1966;2:1113–1115.
27. Jagust WJ, Friedland RP, Budinger TF. Positron emission tomography with [^{18}F]fluorodeoxyglucose differentiates normal pressure hydrocephalus from Alzheimer-type dementia. *J Neurol Neurosurg Psych* 1985;48:1091–1096.
28. Frost JJ. Receptor imaging by positron emission tomography and single-photon emission computed tomography. *Investigative Rad* 1992;27(suppl 2):S54–S58.
29. Kashimada A, Machida K, Honda N, et al. Evaluation of ^{123}I-iomazenil SPECT for cerebrovascular disease: comparison with brain perfusion SPECT and brain MRI [Abstract]. *Nuklearmedizin* 1996;10:S119.